Annals of Botany **114**: 1779–1787, 2014
doi:10.1093/aob/mcu200, available online at www.aob.oxfordjournals.org

ANNALS OF BOTANY Founded 1887

TECHNICAL ARTICLE

A multi-imaging approach to study the root–soil interface

Nicole Rudolph-Mohr[1,*], Peter Vontobel[2] and Sascha E. Oswald[1]

[1]*Institute of Earth and Environmental Science, University of Potsdam, Karl-Liebknecht-Str. 24–25, 14476 Potsdam, Germany and* [2]*Paul Scherrer Institute, 5232 Villigen, Switzerland*
** For correspondence. E-mail nrudolph@uni-potsdam.de*

Received: 26 June 2014 Returned for revision: 23 July 2014 Accepted: 26 August 2014 Published electronically: 25 October 2014

• **Background and Aims** Dynamic processes occurring at the soil–root interface crucially influence soil physical, chemical and biological properties at a local scale around the roots, and are technically challenging to capture *in situ*. This study presents a novel multi-imaging approach combining fluorescence and neutron radiography that is able to simultaneously monitor root growth, water content distribution, root respiration and root exudation.
• **Methods** Germinated seeds of white lupins (*Lupinus albus*) were planted in boron-free glass rhizotrons. After 11 d, the rhizotrons were wetted from the bottom and time series of fluorescence and neutron images were taken during the subsequent day and night cycles for 13 d. The following day (i.e. 25 d after planting) the rhizotrons were again wetted from the bottom and the measurements were repeated. Fluorescence sensor foils were attached to the inner sides of the glass and measurements of oxygen and pH were made on the basis of fluorescence intensity. The experimental set-up allowed for simultaneous fluorescence imaging and neutron radiography.
• **Key Results** The interrelated patterns of root growth and distribution in the soil, root respiration, exudation and water uptake could all be studied non-destructively and at high temporal and spatial resolution. The older parts of the root system with greater root-length density were associated with fast decreases of water content and rapid changes in oxygen concentration. pH values around the roots located in areas with low soil water content were significantly lower than the rest of the root system.
• **Conclusions** The results suggest that the combined imaging set-up developed here, incorporating fluorescence intensity measurements, is able to map important biogeochemical parameters in the soil around living plants with a spatial resolution that is sufficiently high enough to relate the patterns observed to the root system.

Key words: Roots, soil–root interaction, root distribution, *Lupinus albus*, lupin, pH dynamics, oxygen dynamics, soil water distribution, rhizosphere, fluorescence imaging, neutron radiography.

INTRODUCTION

A variety of non-invasive imaging techniques are utilized for the measurement of the distribution of biogeochemical parameters in plant–soil systems. Imaging methods used in plant science are optical imaging using visible light, X-ray computed tomography (CT; Flavel *et al*., 2012; Verboven *et al*., 2012), neutron radiography (NR) and tomography, and magnetic resonance imaging (MRI; Moradi *et al*., 2008). MRI is a powerful tool not only to study the spatial distribution of water, roots and dissolved ions in soils, but also provides information on transport processes (Amin *et al*., 1998; Pohlmeier *et al*., 2008; Moradi *et al*., 2010). However, the presence of paramagnetic compounds inherent in natural soils limits the application of MRI to soil–plant systems to carefully selected porous media (Moradi *et al*., 2008). X-ray CT, by contrast, is less sensitive in detecting plant roots due to small density differences between soil matrix and plant roots (Zappala *et al*., 2013), although it is favourable for investigating soil structure and pore geometry (Mooney *et al*., 2012). X-ray CT was applied to study the formation of gaps around lupin roots as a result of water limitation to the plant (Carminati *et al*., 2009), root growth and soil moisture development around the roots as they grow (Pierret *et al*., 2003). Recently, Flavel *et al*. (2012) showed the accuracy of X-ray CT to study root length measurement and analysed root system architecture as a function of phosphorous application. The most recent and sensitive application to study water relationships at the soil–root interface is NR. The proton (^{1}H nucleus) shows a much larger interaction with neutrons than most other nuclides. In turn, this high sensitivity to hydrous materials makes hydrogen-bearing materials such as water highly visible (Oswald *et al*., 2008). The application range is broad and covers the *in situ* detection of root development in contaminated soils (Menon *et al*., 2007), the visualization of water flow in small plants from roots via steam to leaf (Matsushima *et al*., 2009) and the quantification of local root water uptake (Zarebanadkouki *et al*., 2012). Recently, Moradi *et al*. (2012) and Carminati (2013) monitored the dynamics of water distribution in the rhizosphere of lupin plants over a period of drying and rewetting. They showed that the rhizosphere's water repellency is not uniform along roots, which impacts the hydraulic conductivity of the rhizosphere.

Optical chemical sensors have been utilized for environmental studies with increasing success during the last decade (Stich *et al*., 2010). Optical sensor materials consist of a dye incorporated in a polymeric matrix to produce a thin sensing foil. A large number of dyes exist, specifically sensitive to monitor changes in pH and oxygen. Favourable sensor dye properties are high chemical stability (Carraway *et al*., 1991*a*), high quantum yields (Amao and Okura, 2000), and fast response and recovery times (Mills and Lepre, 1997). The choice of

fluorescent dyes and polymeric matrices strongly influences the sensitivity of the corresponding sensor. Hulth *et al.* (2002) incorporated HPTS (8-hydroxypyrene-1,3,6-trisulfonic acid) into cellulose acetate resulting in a pH range 6·5–8·5 whereas Stahl *et al.* (2006) obtained a dynamic range between pH ≈7·3 and 9·3 by using a fluorescein derivative attached to a hydrogel. The same is true for oxygen sensors, with a sensitivity range of 0–100 % oxygen if a palladium porphyrin complex is embedded into poly(styrene-co-acrylonitrile) (Borisov *et al.*, 2006) and 0–0·005 % if fullerene is incorporated into organosilica (Baleizao *et al.*, 2008). Optical sensors have been developed for a variety of important environmental analytes such as pH, O_2, NH_4^+, CO_2, temperature and various ionic species (Weidgans *et al.*, 2004; Schröder *et al.*, 2007*b*; Baleizao *et al.*, 2008; Strömberg, 2008). The few reports on spatial and temporal patterns of rhizosphere dynamics include the mapping of ammonium turnover in tomato plants (Strömberg, 2008), pH distribution in the rhizosphere of soft-rush (Blossfeld and Gansert, 2007) and lupin plants (Rudolph *et al.*, 2013), and oxygen leakage into the rhizosphere of seagrass (Frederiksen and Glud, 2006).

Key biological functions of plant roots such as water and nutrient uptake, respiration, and exudation alter the concentrations of nutrients, toxic elements and pollutants, pH, redox potential, and partial pressure of O_2 and CO_2 in their rhizosphere (Hinsinger *et al.*, 2005). The extent of the rhizosphere is influenced strongly by root activity, meaning the radial extension of the rhizosphere can range from sub-micrometre to supra-centimetre (Gregory, 2006). Consequently, the soil–root interface is complex and highly heterogeneous in space and time. Therefore, understanding the response of plants to their environments requires tools capable of capturing both spatial and temporal resolution of biogeochemical parameters. Neumann *et al.* (2009) postulated the major challenges of plant sciences in rhizosphere research, which included the *in situ* detection and quantification of root distribution and the monitoring of root activities, reflected by root-induced physicochemical changes in the rhizosphere.

Root-mediated processes are strongly correlated; for example, elevated CO_2 values can result from both root respiration and root exudation (Hinsinger *et al.*, 2003). Tournaire-Roux *et al.* (2003) showed that oxygen-limiting conditions increased cytoplasmic pH, which in turn reduced the conductivity of aquaporins involved in root water uptake. Recent advances in technology have made it possible to visualize and quantify two rhizosphere parameters simultaneously. Blossfeld *et al.* (2013) monitored simultaneously pH and CO_2 dynamics around roots of wheat, chickpea and Australian native broom (*Viminaria juncea*). Schreiber *et al.* (2012) reported strongest rhizospheric acidification and oxygen release at the root tip and root-elongation zone of two flooded plant species. Rudolph *et al.* (2012) pointed out the need to study simultaneously water and oxygen dynamics in the rhizosphere of lupin plants.

The present work introduces and applies a novel multi-imaging approach that is able to simultaneously monitor root growth, water content distribution, root respiration and root exudation. The combination of NR and fluorescence imaging using optical sensors allows *in situ* quantification of the interrelated pattern of water content, oxygen consumption and pH changes at high spatial and temporal resolution. Because of the interrelation between water content distributions, oxygen consumption and pH distribution, NR perfectly complements the fluorescence imaging, targeting chemical parameters by use of specific optical sensor materials. NR is the only means to visualize the roots and to quantify soil water content at the same time. For the first time, we are able to visualize three important biogeochemical parameters, in addition to root structure itself, at the soil–root interface with high spatial and temporal resolution. The approach presented provides insight into the undisturbed, interrelated pattern of root respiration, root exudation, root distribution and root water uptake.

MATERIAL AND METHODS

Plant growth

White lupins (*Lupinus albus*) were grown in boron-free glass rhizotrons with internal dimensions of 0·15 × 0·15 × 0·015 m (see Fig. 1, left image). The inner-sides of the rhizotron were equipped with oxygen- and pH-sensitive foils which covered an area of 0·12 × 0·14 m. The quasi-2-D design was chosen to increase contrasts between soil and water, and to reduce noise and scattering in neutron radiographies and hence to allow quantification of water (Hassanein, 2006). Thus, the experimental design was a compromise between good growing conditions for the plants and optimal visualization conditions for the applied imaging methods. To avoid layering, all rhizotrons were filled horizontally with a homogenous quartz sand mixture characterized by a grain size distribution of 200–2000 μm. A layer of finer sand (grain size distribution 1–250 μm, clay layer) was built in the vertical centre of the containers to prevent quick gas exchange between the lower compartment and the atmosphere. The bottom of the rhizotrons was prepared with holes to allow wetting by capillary forces. To prevent loss of soil material during experiments a gauze was attached. Considering water balance and oxygen exchange, we sealed the bottom wall using aluminium tape after saturation events. To minimize evaporation, we covered the soil surface in each container with a 1-cm-thick layer of coarse gravel. To prevent photobleaching of the sensor dye and light interference with root growth and function, all containers were covered with dark cardboard which was only removed during the particular imaging procedures. Plants were grown in a mobile plant growth cabinet (Vötsch, Balingen, Germany) located directly in the facility hall at Paul Scherer Institute (PSI), Villigen, Switzerland. Daily photoperiod was 14 h (0600–2000h), day temperature was 25 °C and night temperature was 19 °C, with constant relative humidity of 60 %. One single germinated seed was placed into each container and irrigated for the first 10 d from the top of the container. Then, containers were wetted from the bottom. After this irrigation event, we simultaneously took neutron radiographs and fluorescence images during day and night cycles to image root growth, soil water content as well as pH and oxygen dynamics during the following 13 d. On day 14, this procedure was repeated.

Fluorescence sensor imaging

According to Fuller *et al.* (2003), optical response depends on fluorescence intensity, lifetime and spectral distributions. Our

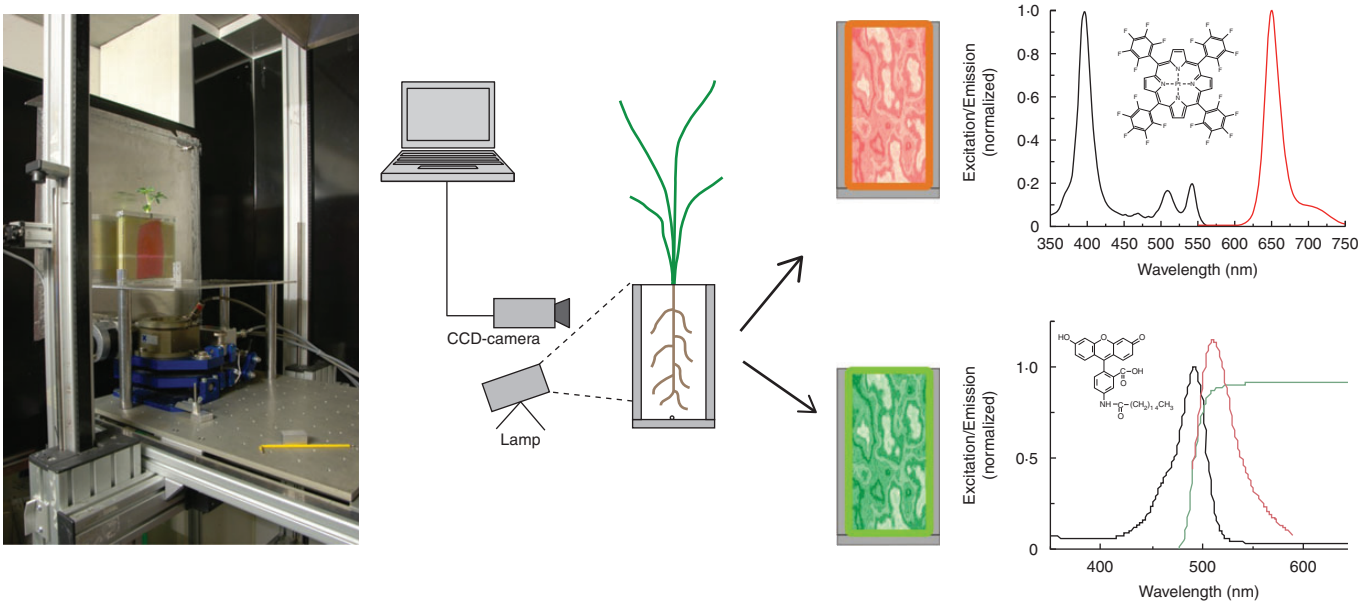

FIG. 1. Image of the neutron imaging setup inside the shielded area (left) and sketch of the fluorescence imaging setup and its detection principles (right).

novel approach using an intensity-based measurement has the advantage of mapping larger areas in shorter times, and uses low-cost equipment (Rudolph *et al.*, 2012). It also allows a mobile and quick setup for experiments with a relatively large number of replicates. Only a few reports on the spatial and temporal patterns of the rhizosphere using an intensity-based fluorescence imaging setup exist in the literature. These include the work of Frederiksen and Glud (2006) and Jensen *et al.* (2005) studying oxygen dynamics in the rhizosphere of *Zostera marina*. The benefits of intensity-based measurements are two-fold: (1) a broad range of possible sensor dyes that have a large Stokes' shift, which means that the absorption/emission signal can be separated spectrally (Borisov *et al.*, 2006); and (2) the visible excitation/response spectra of those sensor dyes that allow (Fuller *et al.*, 2003) the use of inexpensive optics (CCD camera) and light sources (UV lamp) to obtain quantitative values with a high spatial and temporal resolution. The advantage of lifetime measurements is that they are self-referenced, but this necessitates a complex, expensive experimental setup and only a limited numbers of dyes are suitable (Stich *et al.*, 2010). Studies based on lifetime measurements include the work of Blossfeld *et al.* (2011) and Schreiber *et al.* (2012) monitoring pH, oxygen and organic acid dynamics in the rhizosphere of wetland plants.

Oxygen imaging

The sensing scheme for oxygen is based on the ability of oxygen to act as a fluorescence quencher, which means that oxygen decreases the fluorescence yield (Carraway *et al.*, 1991*a*). Therefore, the sensor layer in oxygen-free water shows the strongest fluorescence intensity I_0. The quenching effect is a function of temperature and oxygen concentration (Baleizao *et al.*, 2008). At constant temperature the Stern–Vollmer plot shows non-linear behaviour (Carraway *et al.*, 1991*b*). However, it has been shown that oxygen probes dissolved in polystyrene can be described by a slightly adapted Stern–Vollmer equation (Klimant *et al.*, 1995):

$$\frac{I_0}{I} = \left[\frac{f}{1 + K_{SV}[O_2]} + (1 - f)\right]^{-1} \quad (1)$$

where I_0 is the fluorescence intensity in oxygen-free water, I is fluorescence intensity, K_{SV} is the Stern–Vollmer constant, $[O_2]$ is oxygen concentration, and f is the quenchable and $(1-f)$ is the non-quenchable fraction of the fluorescent dye. K_{SV} depends only on the composition of the sensing layer, characterizes the sensitivity of the resulting sensor and remains constant for a defined sensor composition (Klimant *et al.*, 1995).

Preparation and calibration of oxygen sensing matrix. The oxygen sensor was prepared according to Rudolph *et al.* (2012). In short, 0·2 g platinum (II) 5,10,15,20-tetrakis(2,3,4,5,6-pentafluorophenyl)porphyrin (http://www.porphyrin-systems.de/), 1·98 g polystyrene (Sigma-Aldrich, Munich, Germany) and 18 g toluene (Sigma-Aldrich) were dissolved and knife-coated onto a 50-μm polyester support (Melinex, 506, http://www.puetz-folien.com). After solvent evaporation in ambient air, the resulting thickness was approximately 10 μm. Calibration of the sensor was performed at room temperature (21 °C). Before the main experiment, we conducted the calibration experiment by flushing the container with water of different oxygen concentrations. Oxygen-free water was prepared using sodium dithionite (Merck Millipore, Darmstadt, Germany). A recalibration was done after the experiments were finished. Figure 2B shows the calibration at the beginning of the experiments and the recalibration curve of the oxygen sensor. The oxygen sensor shows highest sensitivity between 0 and 5 mg L^{-1} but is still applicable up to 10 mg L^{-1}.

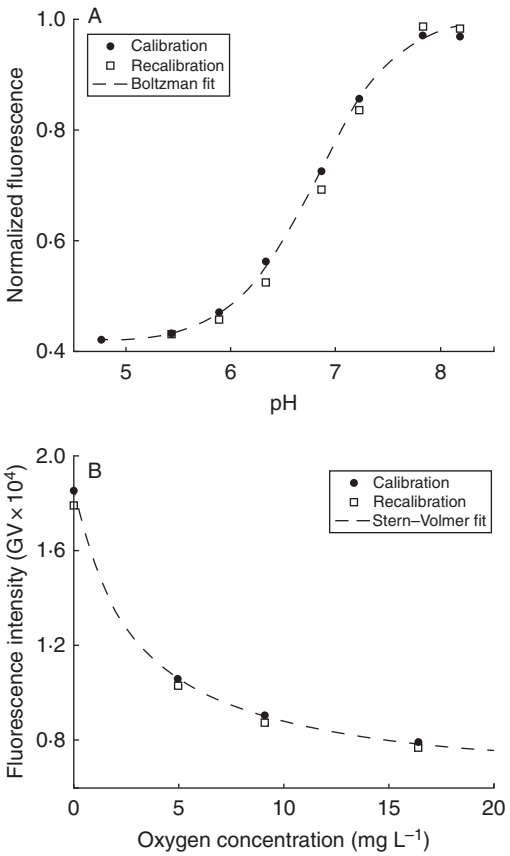

FIG. 2. Calibration and recalibration of the produced sensors: (A) pH, (B) oxygen.

pH imaging

The signal in most optical pH sensors is based on the change in the spectral properties of an acid/base conjugate pair of the pH indicator and the permeation selectivity provided by the polymeric matrix (Weidgans *et al.*, 2004). The cross-sensitivity of pH sensors to temperature (Borisov *et al.*, 2011) and ionic strength (Schröder *et al.*, 2007*a*) has been investigated. During the experiments presented here, the temperature changed between 19 and 25 °C, where we did not find a significant effect. To minimize ionic strength interference we chose a lipophilic fluorescein derivate as suggested by Weidgans *et al.* (2004). Using the approach of Schröder *et al.* (2007*a*), the normalized fluorescence intensity in the images is related to the pH on the basis of the Boltzmann (sigmoidal) function:

$$\frac{F}{F_0} = \frac{A_1 - A_2}{1 + \exp\left(\dfrac{\mathrm{pH} - \mathrm{p}K'_a}{p}\right)} + A_2 \qquad (2)$$

where F_0 and F are the fluorescence signals measured at maximum pH concentrations during calibration (F_0) and during experiments (F). A_1, A_2, $\mathrm{p}K'_a$ and p are empirical parameters describing the initial value (A_1), the final value (A_2), the point of inflection ($\mathrm{p}K'_a$) and the width of the sigmoidal curve (p) (Schröder *et al.*, 2007*a*). Note that the point of inflection corresponds to the apparent $\mathrm{p}K_a$ value ($\mathrm{p}K'_a$).

Preparation and calibration of pH sensing matrix. The sensor layer was prepared according to Rudolph *et al.* (2013). In short, 1 g of hydrogel (HydroMed D4, AdvanSource Biomaterials, Wilmington, MA, USA) was dissolved in a 9 : 1 ethanol/water mixture. Then, 10 mg of the pH indicator 5-hexadecanoylaminofluorescein (Fisher Scientific, Schwerte, Germany) was added to 1 g hydrogel solution and stirred for 12 h. A knife-coating device (Byko-drive, http://www.byk.com/en) was subsequently used to spread the sensor solution onto a dust-free polyster support (Melinex 505, http://www.puetz-folien.com) and evaporated in ambient air for 24 h. Sensor calibration was performed with acidic ($NaH_2PO_4.H_2O$) and basic ($Na_2HPO_4.2H_2O$) buffer stock solutions. Buffer solutions with a range of pH values were obtained by mixing the two stock solutions. The pH values were validated by measuring the pH via a digital pH meter (WTW, Weilheim, Germany) calibrated by a two-point calibration (pH 7·00 and 4·00). Figure 2A shows the calibration and the recalibration curve of the pH sensor. The normalized fluorescence was plotted against pH and fitted by the Boltzmann function. The point of inflection corresponding to the apparent $\mathrm{p}K_a$ value ($\mathrm{p}K'_a$) is at 6·8 with a dynamic range of 5·3–8·3. Together with the oxygen sensitivity between 0 and 5 mg L^{-1} the chosen sensing system for oxygen and pH covers the range important for physiological applications.

Neutron imaging

NR was performed at the thermal neutron station NEUTRA at the neutron spallation source SINQ at PSI, Villigen, Switzerland. The principle of this imaging technique is that a collimated neutron beam is guided through a sample where the intensity of the flux behind the sample (flux of neutrons that have passed through the sample) is detected by a scintillator plate (neutron detector) and then converted into grey-value images by a CCD camera system. The resulting radiographs contain information about the thickness of the neutron-attenuating components at each location of the sample. The grey values in the images depend on material properties and thus on specific neutron–matter interactions, i.e. neutrons can be absorbed, scattered or undisturbed passing through the sample (Lehmann *et al.*, 1999). From resulting radiograms, water distribution in the sample can be determined after deducting the soil attenuation of neutrons and correcting for artefacts such as background scattering. We did this by using the Monte Carlo-based algorithm 'Quantitative Neutron Imaging' (QNI) software (Hassanein, 2006). According to Hassanein *et al.* (2005), for the corrected images the exponential law of attenuation is valid:

$$-\log\left(\frac{I(x,z,t)}{I_0(x,z)}\right) = \Sigma_{\mathrm{H_2O}} L_{\mathrm{H_2O}}(x,z,t) + \Sigma_{\mathrm{glass}} L_{\mathrm{glass}}(x,z) + \Sigma_{\mathrm{soil}} L_{\mathrm{soil}}(x,z) \qquad (3)$$

where x and z are the horizontal and vertical axis perpendicular to the neutron beam, t is time, $I(x, z, t)$ is the intensity of the transmitted beam and $I_0(x, z, t)$ the intensity of the open beam, Σ_i is the neutron-attenuation coefficient and L_i the thickness of the material, where i represents the material (water, glass or dry soil). We calculated $L_{\mathrm{H_2O}}(x, z, t)$ by rearranging eqn (3)

and calculated the water content $\theta(x, z, t)$ according to Carminati and Flühler (2009):

$$\theta(x, z, t) = \frac{L_{H_2O}(x, z, t)}{L_{tot}(x, z)} \quad (4)$$

where $L_{tot}(x, z)$ is the total thickness of the inner space of the rhizotron. Using this procedure, the root structure in soil can be identified clearly and the water content of the soil can be calculated precisely for all pixels. As soil moisture increased the thickness of the attenuating components, NR is limited at high soil water contents due to increased neutron scattering and at very low soil water content due to root dehydration. However, not only could main roots be detected but so too could laterals $\geq$0·2 mm (Moradi *et al*., 2009). In more detail, Leitner *et al*. (2014) showed that the mean root radius for 12- to 26-d-old lupin plants is 0·7 mm for laterals. Therefore, we assume that most of the roots can be detected. More details can be found in Oswald *et al*. (2008), Moradi *et al*. (2009) and Carminati *et al*. (2010).

Combined imaging setup

To simultaneously investigate pH, oxygen and water dynamics in the rhizosphere at high temporal and spatial resolution, we combined the two non-destructive imaging methods of fluorescence imaging and NR. As shown in Fig. 1, the mobile setup for fluorescence imaging was built inside the shielded area of NEUTRA. The CCD camera and the UV light were installed next to each other in relation to the scintillator plate. A slight offset related to the direction of the neutron beam was considered to protect the camera from radiation and to avoid any disturbance during neutron imaging. To correct this shift, samples were relocated by shifting the rotation table horizontally for a defined distance before fluorescence imaging performance was evaluated.

The field of view of the fluorescence images was 258 × 221 mm, resulting in a pixel resolution of 0·21 mm. Neutron radiographs were taken with a pixel size of 0·09 mm, covering a field of view of 197 × 197 mm. This means that our coupled imaging setup generates images where every pixel yields quantitative information of either O_2, pH or H_2O. For each sample, we took neutron radiographs and directly thereafter fluorescence images covering the whole day–night cycle.

RESULTS AND DISCUSSION

Testing the multi-imaging approach

The suitability of combing fluorescence and neutron imaging can be evaluated from Fig. 3. The corrected neutron radiograph (centre) shows the root structure and water content distribution whereas the left fluorescence image shows the pH distribution and the right image illustrates the oxygen distribution around the roots of the same living lupin. The sensor foils cover the main part of the root system (red frame in the centre figure) including tap root and lateral roots (see Fig. 3). The combined setup enables us to relate observed patchy oxygen and pH patterns to specific root parts. Moreover, NR (Fig. 3, centre) can be used to segment the roots. The roots were segmented using the SmartRoot tool of ImageJ (Lobet *et al*., 2011). We could not segment the roots inside the clay layer because of the high water content and resulting strong attenuation of the neutron beam. This makes it impossible to distinguish between roots and water in this layer.

Fluorescence imaging revealed signal changes in oxygen or pH distributions of the roots growing along the sensing foils, as highlighted in Fig. 3. However, the benefit of combining fluorescence imaging and NR is that we can visualize not only the roots growing on the face of the container walls but also the roots inside the opaque soil. This makes it easy to relate observed patterns of oxygen and pH to entire roots. By superimposing the segmented roots from NR on top of the fluorescence images we were able to highlight that acidification occurs locally around the roots (Fig. 4B, lower compartment). Figure 4B also shows

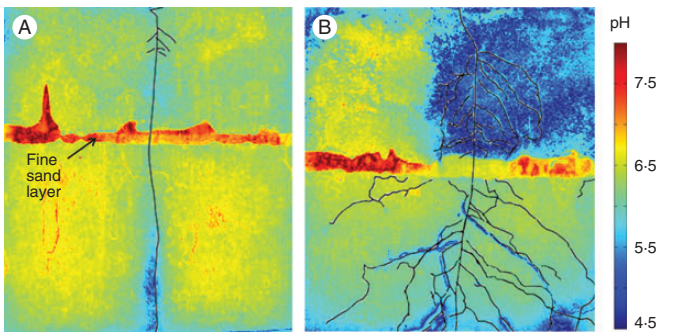

FIG. 4. pH distribution in a soil planted with lupin (A, 5 d old; B, 21 d old) and the overlying segmented roots from NR.

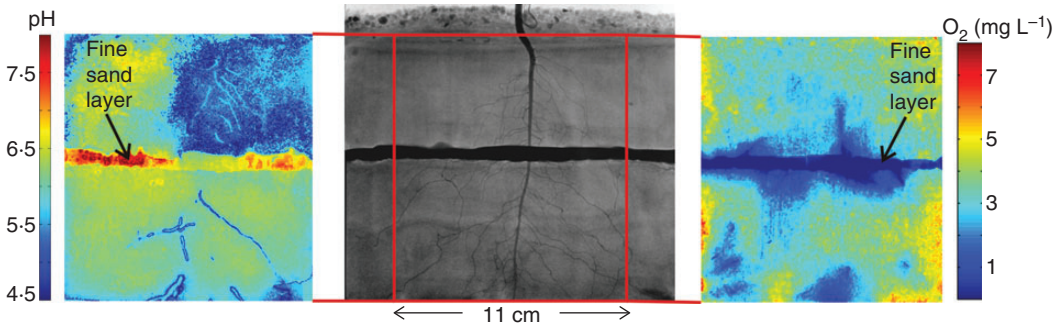

FIG. 3. Container with white lupin in a quartz sand captured by NR (corrected raw images, centre), and the same container through fluorescence O_2-sensitive foil (right) and pH-sensitive foil (left).

the influence of high root density on pH dynamics. The acidification in the upper compartment is limited to the location of the dense root network.

The sensitivity of the sensing foils is shown in more detail in Fig. 4A. The root system of a 5-d-old lupin consists mainly of the tap root and thus it is possible only in the upper part of the container to identify first lateral roots. The pH image reveals acidification limited in spatial extent to the position of the tap root. The thickness of the soil in the container is 1·5 cm. This means the sensing foils responded to signal changes in the soil up to 0·75 cm deep inside the soil.

Oxygen, pH and water content distribution around plant roots

On the basis of the resulting root mask, various calculations on root characteristics can be performed, for example root thickness or root length. We calculated total root length of a white lupin (Fig. 5, left) that nearly doubled from 972·42 mm on day 11 to 1801·51 mm on day 25. In the lower compartment below the fine sand layer, root length increased from 587·5 to 1300·3 mm. The oxygen images of the same root systems (Fig. 5) show oxygen deficit zones developing below the fine sand layer after watering. The rhizotron was watered from the bottom by capillary rise. Overlaying the segmented roots from NR on top of the fluorescence images, we observed that the oxygen deficits occur around the roots. Figure 5 demonstrates the time series of oxygen patterns for two lupin root systems of different age. The 25-d-old root system shows very strong oxygen depletion within the first 10 h after watering. After 24 h, we observed oxygenation in the upper compartment. The lower compartment with a root length of 1300·3 mm oxygen depletion expands from a local pattern to a diffuse extent that covers the complete compartment. The high water content in the fine sand layer limits the downward diffusion of atmospheric oxygen. Due to ongoing respiration activity, high water content and limited oxygen exchange between the lower compartment and the atmosphere, the anoxic zone develops to values below 0·1 mg L^{-1}. During the following 24 h, the oxygen depletion zones almost disappear. Transpiration activity consequently reduces the water content within the bottom compartment. Subsequently, the ongoing respiration and transpiration activity result in the recovery of connected air phase and exchange between atmospheric oxygen and soil pores in the bottom compartment.

The 11-d-old root system has a total root length of 972·42 mm, with 587·5 mm in the bottom compartment. Within the first 48 h anoxic zones decreased slowly below 0·5 mg L^{-1}. The maximum extent of oxygen depletion is reached after 48 h but the anoxic conditions remain stable during the next 24 h. This is comparison to the 25-d-old root system where the higher root length resulted in higher root water uptake rates and thus faster water extraction. Average water loss in the older root system was 1·2 g h^{-1} during the photoperiod whereas the young root system had a water uptake during daytime of 0·6 g h^{-1}. The water uptake rates contrast with those reported by Carminati *et al.* (2010) who investigated changes in soil water content in the rhizosphere of lupin plants.

Figure 6 highlights the soil pH and soil water content around a single lupin root as a function of distance from the root centre. The root can be clearly detected by means of a pH decrease of more than 1 pH unit compared with bulk soil pH. A steep pH gradient (pH 5·00–6·15) was observed at the soil–root interface ($\leq$1 mm), whereas in soil further from the root (1–4 mm) the pH rose slightly from 6·15 to 6·70. In addition, roots can be distinguished from the surrounding soil by the sharp increase in water content compared with soil. A similar pattern of root-induced changes in soil pH mainly restricted to the rhizosphere was reported for soft-rush (Blossfeld and Gansert,

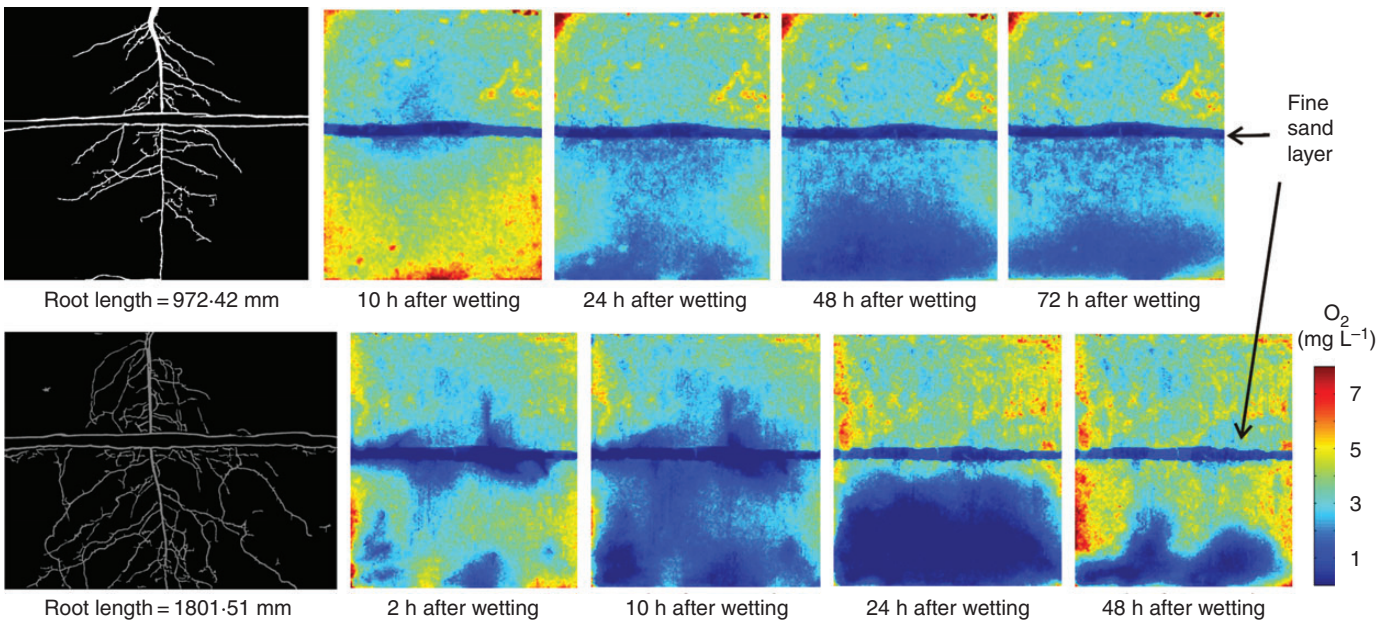

FIG. 5. Segmented roots and the corresponding time series of oxygen depletion which develops after wetting in 25-d-old white lupin (top) and 11-d-old white lupin (bottom).

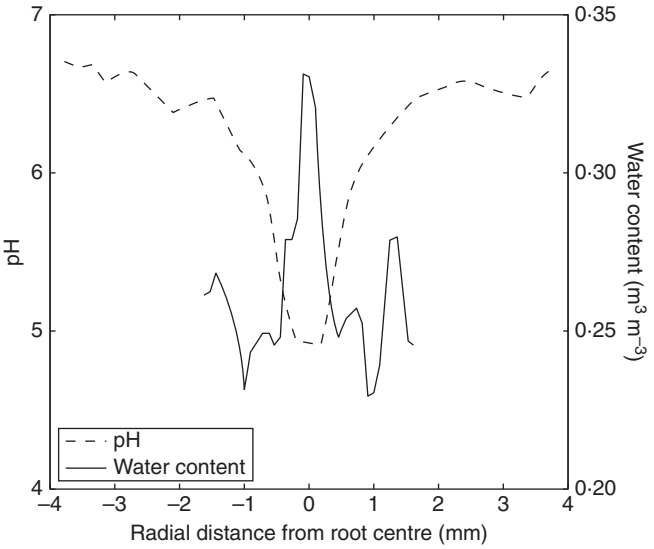

FIG. 6. Soil pH and water content profiles around a single root of white lupin plotted against distance from the root centre.

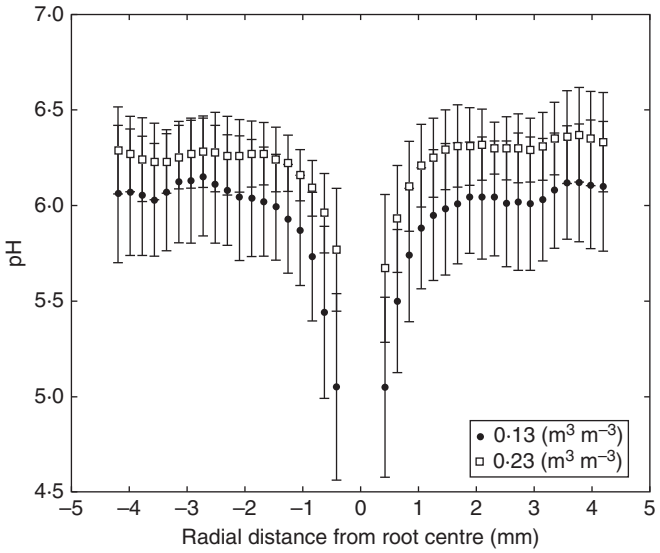

FIG. 7. Soil pH profiles around the roots of lupin plants as the mean of 12 laterals with standard deviations as a function of distance from the root centre at different water contents. Increased water content produces significantly higher pH values around the roots (*t*-test; $P < 0{\cdot}05$).

2007) and maize (Jaillard *et al*., 1996; Plassard *et al*., 1999). Dessureault-Rompré *et al*. (2006) observed a steep pH decrease ($\approx 2{\cdot}5$ pH units) in the vicinity of white lupin due to an exudative burst of organic acid anions, for example citrate or malate. Marschner and Römheld (1983) showed that pH changes in the rhizosphere of plants depend on initial bulk soil pH and nitrogen fertilization; for example, maize fertilized with NO_3^--N increased bulk soil pH from 6·0 to 7·5 whereas bulk soil pH dropped to about 4 with NH_4^+-N as nitrogen supply (Marschner and Römheld, 1983).

The above calculations were repeated in the soil pH profiles of 12 different lateral roots and two different water contents (relatively dry with $\theta = 0{\cdot}13$ m^3 m^{-3} and relatively wet with $\theta = 0{\cdot}23$ m^3 m^{-3}) were taken into account. Statistical analysis was run at a confidence level of 95 %. As shown in Figure 7, for both water contents, soil pH was more acidic directly at the soil–root interface (distances of $\leq$1 mm from root) than in the more distal soil (1–5 mm), i.e. soil pH rose from 5·05 to 6·30 with increasing radial distance from the root. Furthermore, higher soil water contents consequently resulted in increased pH values where the difference in pH was highest at the soil–root interface (0·3 pH units versus 0·1 pH units). A temporal increase of rhizosphere pH after irrigation followed by a subsequent decrease of pH has been also observed by Schreiber *et al*. (2012) and Blossfeld *et al*. (2013). Thus, we observed a strong interrelationship between θ and pH and a spatial variability of root acidification depending on radial distance to the root centre. The spatial distribution of rhizosphere acidification indicates that lower pH values at the soil–root interface are caused by root activities. Root-induced changes in soil pH can results from, for example, root respiration, compensation for cation–anion exchange balance, root exudation, and environmental or nutritional constraints (Marschner and Römheld, 1994; Nichol and Silk, 2001; Hinsinger *et al*., 2003). Few data relating soil water content and pH increase are available. Based on his modelling approach, Nye (1981) postulated a high sensitivity of pH changes to soil water content. Thus, our observed pH dynamics could be directly linked to increased soil moisture. Reduced proton diffusion rates in dry soils as described by Olesen *et al*. (2000) and Nichol and Silk (2001) are a possible explanation for pH variations with soil moisture contents. Another explanation might be related to increased root activities during dry conditions such as higher H^+ release (Riley and Barber, 1969; Jaillard *et al*., 2002) or root exudation rates (Nye, 1981; Haynes, 1990; Marschner and Römheld, 1994; Jaillard *et al*., 2002) both of which are known to decrease rhizosphere pH. However, to verify the dominant process, further research in addition to this specific case study is required.

CONCLUSIONS

We present a novel multi-imaging approach that is able to simultaneously record the dynamics of rhizosphere pH, water content and oxygen distributions with high spatial and temporal resolution. The combination of NR with fluorescence imaging enables us to relate observed changes in soil pH and oxygen levels to root structure and soil water content. The advantage of using NR is the relatively high throughput and the strong contrast between soil and roots that requires little effort in image processing. The advantage of fluorescence imaging is its high adaptability. Studies have described fluorescence dyes sensitive to, for example, CO_2, ammonium and temperature. Our novel multi-imaging approach uses fluorescence sensors sensitive to pH and oxygen with a high stability, regulated by the choice of the sensor dye.

By superimposing the segmented roots from NR on top of the fluorescence images we were able to highlight three important biogeochemical parameters in the rhizosphere of plants. The observed oxygen pattern shows that during an irrigation event the young root system has to cope with longer periods of anoxia. The older root systems with increased root length and therefore higher root water uptake show much faster re-aeration.

Because for high soil water contents the contrast between roots and soil becomes less, one aspect of the current experimental setup remains the comparison between root density in oxygen-rich and oxygen-poor conditions. We observed a strong interrelationship between θ and pH but further research is required to clarify if the more pronounced decrease in pH at lower water content is due to increased root activity or reduced proton diffusion rates or something else. It has been demonstrated that this combined setup represents a robust tool for gaining detailed information on the rhizosphere of living plants.

ACKNOWLEDGEMENTS

We acknowledge funding from the German DFG priority programme 1315 'Biogeochemical interfaces in soil', under contract OS 351/1-2.

LITERATURE CITED

Amao Y, Okura I. 2000. An oxygen sensing system based on the phosphorescence quenching of metalloporphyrin thin film on alumina plates. *Analyst* **125**: 1601–1604.

Amin MHG, Hall LD, Chorley RJ, Richards KS. 1998. Infiltration into soils, with particular reference to its visualization and measurement by magnetic resonance imaging (MRI). *Progress in Physical Geography* **22**: 135–165.

Baleizao C, Nagl S, Schaferling M, Berberan-Santos MN, Wolfbeis OS. 2008. Dual fluorescence sensor for trace oxygen and temperature with unmatched range and sensitivity. *Analytical Chemistry* **80**: 6449–6457.

Blossfeld S, Gansert D. 2007. A novel non-invasive optical method for quantitative visualization of pH dynamics in the rhizosphere of plants. *Plant Cell and Environment* **30**: 176–186.

Blossfeld S, Gansert D, Thiele B, Kuhn AJ, Losch R. 2011. The dynamics of oxygen concentration, pH value, and organic acids in the rhizosphere of *Juncus* spp. *Soil Biology & Biochemistry* **43**: 1186–1197.

Blossfeld S, Schreiber CM, Liebsch G, Kuhn AJ, Hinsinger P. 2013. Quantitative imaging of rhizosphere pH and CO_2 dynamics with planar optodes. *Annals of Botany* **112**: 267–276.

Borisov SM, Vasylevska AS, Krause C, Wolfbeis OS. 2006. Composite luminescent material for dual sensing of oxygen and temperature. *Advanced Functional Materials* **16**: 1536–1542.

Borisov SM, Seifner R, Klimant I. 2011. A novel planar optical sensor for simultaneous monitoring of oxygen, carbon dioxide, pH and temperature. *Analytical and Bioanalytical Chemistry* **400**: 2463–2474.

Carminati A. 2013. Rhizosphere wettability decreases with root age: a problem or a strategy to increase water uptake of young roots? *Frontiers in Plant Science* **4**: 298.

Carminati A, Flühler H. 2009. Water infiltration and redistribution in soil aggregate packings. *Vadose Zone Journal* **8**: 150–157.

Carminati A, Vetterlein D, Weller U, Vogel HJ, Oswald SE. 2009. When roots lose contact. *Vadose Zone Journa*, **8**: 805–809.

Carminati A, Moradi AB, Vetterlein D, *et al*. 2010. Dynamics of soil water content in the rhizosphere. *Plant and Soil* **332**: 163–176.

Carraway ER, Demas JN, Degraff BA. 1991*a*. Luminescence quenching mechanism for microheterogeneous systems. *Analytical Chemistry* **63**: 332–336.

Carraway ER, Demas JN, DeGraff BA, Bundt M. 1991*b*. Photophysics and photochemistry of oxygen sensors based on luminescent transition-metal-complexes. *Analytical Chemistry* **63**: 337–342.

Dessureault-Rompre J, Nowack B, Schulin R, Luster J. 2006. Modified micro suction cup/rhizobox approach for the in-situ detection of organic acids in rhizosphere soil solution. *Plant and Soil* **286**: 99–107.

Flavel RJ, Guppy CN, Tighe M, Watt M, McNeill A, Young IM. 2012. Non-destructive quantification of cereal roots in soil using high-resolution X-ray tomography. *Journal of Experimental Botany* **63**: 2503–2511.

Frederiksen MS, Glud RN. 2006. Oxygen dynamics in the rhizosphere of *Zostera marina*: a two-dimensional planar optode study. *Limnology and Oceanography* **51**: 1072–1083.

Fuller ZJ, Bare WD, Kneas KA, Xu WY, Demas JN, DeGraff BA. 2003. Photostability of luminescent ruthenium(II) complexes in polymers and in solution. *Analytical Chemistry* **75**: 2670–2677.

Gregory PJ. 2006. Roots, rhizosphere and soil: the route to a better understanding of soil science? *European Journal of Soil Science* **57**: 2–12.

Hassanein RK. 2006. Correction Methods for the Quantitative Evaluation of thermal Neutron Tomography. Dissertation. ETH No. 16809.

Hassanein R, Lehmann E, Vontobel P. 2005. Methods of scattering corrections for quantitative neutron radiography. *Nuclear Instruments and Methods in Physics Research Section A: Accelerators, Spectrometers, Detectors and Associated Equipment* **542**: 353–360.

Haynes RJ. 1990. Active ion uptake and maintenance of cation-anion balance: a critical examination of their role in regulating rhizosphere pH. *Plant and Soil* **126**: 247–264.

Hinsinger P, Plassard C, Tang CX, Jaillard B. 2003. Origins of root-mediated pH changes in the rhizosphere and their responses to environmental constraints: a review. *Plant and Soil* **248**: 43–59.

Hinsinger P, Gobran GR, Gregory PJ, Wenzel WW. 2005. Rhizosphere geometry and heterogeneity arising from root-mediated physical and chemical processes. *New Phytologist* **168**: 293–303.

Hulth S, Aller RC, Engstrom P, Selander E. 2002. A pH plate fluorosensor (optode) for early diagenetic studies of marine sediments. *Limnology and Oceanography* **47**: 212–220.

Jaillard B, Ruiz L, Arvieu JC. 1996. pH mapping in transparent gel using color indicator videodensitometry. *Plant and Soil* **183**: 85–95.

Jaillard B, Plassard C, Hinsinger P. 2002. Measurement of H^+ fluxes and concentrations in the rhizosphere. In: Rengel Z, ed. *Handbook of soil acidity*. New York: Marcel Dekker, 231–266.

Jensen SI, Kuhl M, Glud RN, Jorgensen LB, Prieme A. 2005. Oxic microzones and radial oxygen loss from roots of *Zostera marina*. *Marine Ecology-Progress Series* **293**: 49–58.

Klimant I, Meyer V, Kuhl M. 1995. Fiberoptic oxygen microsensors, a new tool in aquatic biology. *Limnology and Oceanography* **40**: 1159–1165.

Lehmann E, Pleinert H, Williams T, Pralong C. 1999. Application of new radiation detection techniques at the Paul Scherrer Institut, especially at the spallation neutron source. *Nuclear Instruments & Methods in Physics Research Section a-Accelerators Spectrometers Detectors and Associated Equipment* **424**: 158–164.

Leitner D, Felderer B, Vontobel P, Schnepf A. 2014. Recovering root system traits using image analysis exemplified by two-dimensional neutron radiography images of lupine. *Plant Physiology* **164**: 24–35.

Lobet G, Pages L, Draye X. 2011. A novel image-analysis toolbox enabling quantitative analysis of root system architecture. *Plant Physiology* **157**: 29–39.

Marschner H, Römheld V. 1983. *In vivo* measurement of root-induced pH changes at the soil-root interface: effect of plant species and nitrogen source. *Zeitschrift für Pflanzenphysiologie* **111**: 241–251.

Marschner H, Römheld V. 1994. Strategies of plants for acquisition of iron. *Plant and Soil* **165**: 261–274.

Matsushima U, Herppich WB, Kardjilov N, Graf W, Hilger A, Manke I. 2009. Estimation of water flow velocity in small plants using cold neutron imaging with D_2O tracer. *Nuclear Instruments & Methods in Physics Research Section a-Accelerators Spectrometers Detectors and Associated Equipment* **605**: 146–149.

Menon M, Robinson B, Oswald SE, *et al*. 2007. Visualization of root growth in heterogeneously contaminated soil using neutron radiography. *European Journal of Soil Science* **58**: 802–810.

Mills A, Lepre A. 1997. Controlling the response characteristics of luminescent porphyrin plastic film sensors for oxygen. *Analytical Chemistry* **69**: 4653–4659.

Mooney SJ, Pridmore TP, Helliwell J, Bennett MJ. 2012. Developing X-ray computed tomography to non-invasively image 3-D root systems architecture in soil. *Plant and Soil* **352**: 1–22.

Moradi AB, Oswald SE, Massner JA, Pruessmann KP, Robinson BH, Schulin R. 2008. Magnetic resonance imaging methods to reveal the real-time distribution of nickel in porous media. *European Journal of Soil Science* **59**: 476–485.

Moradi AB, Conesa HM, Robinson B, *et al*. 2009. Neutron radiography as a tool for revealing root development in soil: capabilities and limitations. *Plant and Soil* **318**: 243–255.

Moradi AB, Oswald SE, Nordmeyer-Massner JA, Pruessmann KP, Robinson BH, Schulin R. 2010. Analysis of nickel concentration profiles around the roots of the hyperaccumulator plant *Berkheya coddii* using MRI and numerical simulations. *Plant and Soil* **328**: 291–302.

Moradi AB, Carminati A, Lamparter A, *et al*. 2012. Is the rhizosphere temporarily water repellent? *Vadose Zone Journal* **11**. doi:10.2136/vzj2011.0120.

Neumann G, George TS, Plassard C. 2009. Strategies and methods for studying the rhizosphere – the plant science toolbox. *Plant and Soil* **321**: 431–456.

Nichol SA, Silk WK. 2001. Empirical evidence of a convection-diffusion model for pH patterns in the rhizospheres of root tips. *Plant Cell and Environment* **24**: 967–974.

Nye PH. 1981. Changes of pH across the rhizosphere induced by roots. *Plant and Soil* **61**: 7–26.

Olesen T, Moldrup P, Yamaguchi T, Nissen HH, Rolston DE. 2000. Modified half-cell method for measuring the solute diffusion coefficient in undisturbed, unsaturated soil. *Soil Science* **165**: 835–840.

Oswald SE, Menon M, Carminati A, Vontobel P, Lehmann E, Schulin R. 2008. Quantitative imaging of infiltration, root growth, and root water uptake via neutron radiography. *Vadose Zone Journal* **7**: 1035–1047.

Pierret A, Kirby M, Moran C. 2003. Simultaneous X-ray imaging of plant root growth and water uptake in thin-slab systems. *Plant and Soil* **255**: 361–373.

Plassard C, Meslem M, Souche G, Jaillard B. 1999. Localization and quantification of net fluxes of H^+ along maize roots by combined use of pH-indicator dye videodensitometry and H^+-selective microelectrodes. *Plant and Soil* **211**: 29–39.

Pohlmeier A, Oros-Peusquens A, Javaux M, *et al*. 2008. Changes in soil water content resulting from Ricinus root uptake monitored by magnetic resonance Imaging. *Vadose Zone Journal* **7**: 1010–1017.

Riley D, Barber SA. 1969. Bicarbonate accumulation and pH changes at the soybean (*Glycine max* (L.) Merr.) root-soil interface. *Soil Science Society of America Journal* **33**: 905–908.

Rudolph N, Esser HG, Carminati A, *et al*. 2012. Dynamic oxygen mapping in the root zone by fluorescence dye imaging combined with neutron radiography. *Journal of Soils and Sediments* **12**: 63–74.

Rudolph N, Voss S, Moradi AB, Nagl S, Oswald SE. 2013. Spatio-temporal mapping of local soil pH changes induced by roots of lupin and soft-rush. *Plant and Soil* **369**: 669–680.

Schreiber CM, Zeng B, Blossfeld S, *et al*. 2012. Monitoring rhizospheric pH, oxygen, and organic acid dynamics in two short-time flooded plant species. *Journal of Plant Nutrition and Soil Science* **175**: 761–768.

Schröder, Polerecky L, Klimant I. 2007*a*. Time-resolved pH/pO_2 mapping with luminescent hybrid sensors. *Analytical Chemistry* **79**: 60–70.

Schröder CR, Neurauter G, Klimant I. 2007*b*. Luminescent dual sensor for time-resolved imaging of pCO_2 and pO_2 in aquatic systems. *Microchimia Acta* **158**: 205–218.

Stahl H, Glud A, Schröder CR, Klimant I, Tengberg A, Glud RN. 2006. Time-resolved pH imaging in marine sediments with a luminescent planar optode. *Limnology and Oceanography-Methods* **4**: 336–345.

Stich MIJ, Fischer LH, Wolfbeis OS. 2010. Multiple fluorescent chemical sensing and imaging. *Chemical Society Reviews* **39**: 3102–3114.

Strömberg N. 2008. Determination of ammonium turnover and flow patterns close to roots using imaging optodes. *Environmental Science & Technology* **42**: 1630–1637.

Tournaire-Roux C, Sutka M, Javot H, *et al*. 2003. Cytosolic pH regulates root water transport during anoxic stress through gating of aquaporins. *Nature* **425**: 393–397.

Verboven P, Pedersen O, Herremans E, *et al*. 2012. Root aeration via aerenchymatous phellem: three-dimensional micro-imaging and radial O_2 profiles in *Melilotus siculus*. *New Phytologist* **193**: 420–431.

Weidgans BM, Krause C, Klimant I, Wolfbeis OS. 2004. Fluorescent pH sensors with negligible sensitivity to ionic strength. *Analyst* **129**: 645–650.

Zappala S, Mairhofer S, Tracy S, *et al*. 2013. Quantifying the effect of soil moisture content on segmenting root system architecture in X-ray computed tomography images. *Plant and Soil* **370**: 35–45.

Zarebanadkouki M, Kim YX, Moradi AB, Vogel HJ, Kaestner A, Carminati A. 2012. Quantification and modeling of local root water uptake using neutron radiography and deuterated water. *Vadose Zone Journal* **11**. doi:10.2136/vzj2011.0196.